Slc26a9-mediated Cl^- secretion prevents mucus obstruction in Th2-dependent airway inflammation

Pinelopi Anagnostopoulou, Brigitte Riederer, Julia Duerr, Sven Michel, Aristea Binia, Raman Agrawal, Xuemei Liu, Katrin Kalitzki, Fang Xiao, Mingmin Chen, Jolanthe Schatterny, Dorothee Hartmann, Thomas Thum, Michael Kabesch, Manoocher Soleimani, Ursula Seidler, and Marcus A. Mall

Online Supplement

SUPPLEMENTARY MATERIAL

Supplemental Methods

Experimental animals. Mouse breeding was performed at the institute for animal research at Hannover Medical School. Experimental animals were generated from *Slc26a9*$^{+/-}$ breeding pairs on the 129/SVJ background. Offspring were genotyped by PCR of genomic DNA, as previously described (1). 8 to 20 week-old *Slc26a9*$^{-/-}$ mice and wild-type littermates were used for all experiments. Mice were housed under standardized light cycles in IVC cages and had free access to chow and water.

IL-13 instillation. IL-13 or vehicle alone were administered by repeated intratracheal instillation as previously described (2). In brief, mice were anesthetized by inhalation of isoflurane 3% in oxygen and 5 µg of recombinant murine IL-13 (Peprotech) dissolved in 50 µl of PBS containing 0.1% BSA (low endotoxin, Sigma), or an equal volume of vehicle alone, were administered by intratracheal instillation once daily for 3 consecutive days. Endpoint studies were performed 24 h after the last IL-13 instillation.

Electrogenic ion transport measurements. Mice were deeply anesthetized via i.p. injection of a combination of ketamine and xylazine (120 mg/kg and 16 mg/kg respectively) and killed by exsanguination. Airway tissues were dissected using a stereomicroscope as previously described (2;3). In brief, mainstem bronchi were exposed by a median incision of the anterior part of the neck and a sternotomy. Airway tissues were freed from surrounding muscle, vessels and connective tissue by blunt dissection in situ. Next, bronchi were excised, the anterior part with the cartilage rings was cut open longitudinally, the pars membranacea was exposed and tissues were immediately mounted into perfused micro-Ussing chambers with a circular open area of 0.5 mm^2 (2;4). The luminal and basolateral bath was perfused continuously at a rate of 10 ml/min, a solutions of the following composition: 145 mM NaCl, 0.4 mM KH_2PO_4, 1.6 mM K_2HPO_4, 5 mM D-glucose, 1 mM $MgCl_2$, calcium 1.3 mM gluconate.

The pH was adjusted to 7.4. Experiments were performed at 37°C under open-circuit conditions as previously described (2;4). Values for V_{te} were referenced to the serosal side. R_{te} was determined by applying intermittent (1 s) current pulses (ΔI = 0.5 μA) and the equivalent I_{sc} was calculated according to Ohm's law ($I_{sc} = V_{te}/R_{te}$). After an equilibration period of 40 min in the Ussing chamber, basal I_{sc} was determined and amiloride (100 μM, luminal) was added to inhibit electrogenic ENaC-mediated Na^+ absorption. Then, IBMX (100 μM, luminal) and forskolin (1 μM, luminal), and UTP (100 μM, luminal) were added sequentially to induce cAMP-mediated and Ca^{2+}-activated Cl^- secretion, respectively. In a subset of experiments, the CFTR inhibitor $CFTR_{inh}$-172 (20 μM, luminal) (5) and/or bumetanide (100 μM, basolateral), an inhibitor of the basolateral Na^+-K^+-$2Cl^-$ cotransporter (6), were added to amiloride-pretreated tissues in the absence or presence of IBMX/forskolin to block transepithelial Cl^- secretion. In another series of experiments, basal bioelectric properties, and responses to amiloride and IBMX/forskolin were compared in the absence and presence of HCO_3^-. The HCO_3^- containing solution was prepared according to the HCO_3^--free solution except for replacement of 25 mM NaCl with 25 mM $NaHCO_3$, and the solution was gassed continuously with a mixture of 95% O_2 / 5% CO_2, which maintained the pH at 7.4. All bioelectric measurements were performed by an investigator blinded to the genotype and the treatment of the mice. Amiloride, IBMX, forskolin and bumetanide were obtained from Sigma; UTP was obtained from GE Healthcare and $CFTR_{inh}$-172 from Calbiochem. All chemicals were of the highest grade of purity available.

Histology and airway morphometry. Anesthetized mice were killed by exsanguination. Lungs were removed through a median sternotomy, immersion fixed in 4% buffered formalin, and embedded in paraffin. Lungs were sectioned transversally at the level of the proximal intrapulmonary main axial airway near the hilus, and sections were cut at 5 μm and 1.5 μm and stained with H&E or alcian blue periodic acid-Schiff (AB-PAS) as previously described (7). Images were taken with an Olympus IX-71 microscope interfaced with a SIS Colorview I Camera Set (Olympus) using the 10x and 40x objective. For semi-quantitative assessment of

airway mucus obstruction, lung sections were scored for the absence or presence of intraluminal mucus accumulation, as defined by AB-PAS positive material taking up ≥ 10% of the cross-sectional area of the airway lumen. For quantitative stereological assessment of airway mucus obstruction, we used Analysis B image analysis software (Olympus) to determine mucus volume density as previously described (7;8). In brief, the length of the boundary of the airway lumen, as defined by the luminal membrane of the airway epithelium, was measured by the interactive image measurement tool, and the AB-PAS positive surface area within this boundary was measured by phase analysis according to the automatic threshold settings of the software. The volume density of intraluminal airway mucus, representing the volume of airway mucus content per surface area of the airway lumen (nl/mm^2), was determined from the surface area of AB-PAS positive mucus and the length of the luminal membrane of the airway epithelium, as previously described (8;9). The volume density of the airway epithelium was determined as a measure of epithelial hyperplasia (9). Goblet cells were identified by the presence of intra-cellular AB-PAS positive material and numeric cell densities were quantitated by counting epithelial cells per mm of the basement membrane (7). Numeric densities of ciliated and non-ciliated airway cells were assessed on adjacent 1.5 µm sections stained with H&E. Cell-types were distinguished morphologically by light microscopy at a 40-fold magnification, and cell height of individual airway cells was determined from the distance between the basement membrane and the luminal cell membrane using the interactive image measurement tool. All morphometric measurements were performed by an investigator blinded to the genotype and the treatment of the mice.

Real time RT-PCR. Airway tissues were immediately stored in RNA later (Applied Biosystems). RNA was isolated using RNeasy Mini Kit (Qiagen). RNA purity and quantity were determined using the Epoch-Reader and Take3 Multi-Volume-Plate (Biotec Instruments), and integrity was verified by QIAxcel capillary electrophoresis (Qiagen). cDNA was obtained by reverse transcription of 2 µg of total RNA (RevertAid Premium RT; Fermentas). Real-time PCR reactions for Slc26a9 and Gapdh were carried out using

MesaGreen PCR-Master-Mix (Eurogentec) in the Applied Biosystems 7300 Realtime PCR System according to the manufacturer's instructions (Applied Biosystems). PCR extension was performed at 60°C with 40 repeats. Data were analyzed using the Sequence Detection Software 1.2.3 (Applied Biosystems) and exported to Microsoft Excel. Relative quantification of Slc26a9 mRNA expression was calculated from the efficiency of the PCR reaction and the crossing point deviation between samples from vehicle-treated and IL-13 treated wild-type mice, and determined by normalization to expression of the reference gene Gapdh, as previously described (7;10).

Population genetics analysis. The dataset used for the analysis of human variants in the *SCL26A9* gene was derived from our population previously included in the first published genome wide-association study (GWAS) on asthma (11). For this GWAS, two independent study populations have been combined. Asthma cases were derived from the Multicenter Asthma Genetic in Childhood (MAGIC) study. Initially 1255 children were recruited from seven German and Austrian clinical asthma centers and in 865 of them (mean age 11 years) pediatric pulmonologists diagnosed asthma based on physical examinations, clinical history, lung function tests and allergy testing (skin prick testing and serum IgE measurement). Polymorphism selection was based on the HapMap database (http://www.hapmap.org), release#24, phase 1&2 - full dataset/Nov08/on NCBI B36 assembly, dbSNP b126. As previously described (12), 655 children of those were genotyped on the Illumina Sentrix HumanHap300 BeadChip together with 767 randomly selected children (73 asthmatics) from phase II of the ISAAC study. Asthmatic children from the random sample taken from the ISAAC phase II study were treated as asthma cases in the analysis. In this large (n=5629) cross sectional International Study of Asthma and Allergy in Childhood conducted in Munich and Dresden the status of asthma was based on parent's reports (13). Out of all genotyped samples, 1319 (661 asthmatics) passed all subsequent quality controls including an update of consent in a follow up study causing a slight decrease in the number of children from MAGIC contributing to this analysis compared to previous studies (11;12). For the imputation

conducted by Liming Liang a hidden Markov model (MaCH) (14) was used to presume the genotypes for all polymorphic SNPs from HapMap phase II (15). Statistical analyses and quality control were performed with PLINK software package version 1.07. All associations with accompanying odds ratio and confidence intervals were evaluated using an additive regression model. We are grateful to the MAGIC and ISAAC II genetic study groups for providing the dataset for genetic association analysis.

Cloning of *SLC26A9* 3'UTR and luciferase gene reporter assays. A BLASTN search using the microRNA database and target prediction tool miRBase (www.miRBase.org) identified a potential *hsa-miR-632* binding site in the A allele (SNP) of rs2282430 in the 3'UTR of *SLC26A9*. The native *SLC26A9* 3'UTR (2.3 kb) containing the G allele (wild-type) of rs2282430 was cloned into a pCR®2.1-TOPO vector (Invitrogen) and the polymorphic site was mutated to A allele (SNP) using QuickChange™Site-directed mutagenesis kit (Agilent Technologies). The clones containing the wild-type and polymorphic alleles of the *SLC26A9* 3'UTR were subcloned into the pmirGLO vector (Promega). A549 cells (16) (1.5 x 10^5 cells per well) were transfected with 5 µg of pmirGLO constructs containing either the wild-type or polymorphic allele of the *SLC26A9* 3'UTR, or empty pmirGLO vector alone, by the Nucleofector® kit T (Lonza BioResearch). Firefly and Renilla luciferase activity was measured after 24 hr using the Dual-Glo® Luciferase Assay System (Promega), and data were analysed by normalizing firefly luciferase activity to Renilla luciferase activity. These studies showed that the wild-type *SLC26A9* 3'UTR sequence reduced relative luciferase activity substantially compared to the empty vector (pmirGLO) (7.6 $\pm$ 0.3 for empty vector versus 1.0 $\pm$ 0.03 for wild-type *SLC26A9* 3'UTR, n = 10, $P < 0.0001$) demonstrating a prominent regulatory role as shown for 3'UTRs of other genes (17). Targeting of the polymorphic allele of the *SLC26A9* 3'UTR by *hsa-miR-632* was validated in HEK293 cells. HEK293 cells (1.5 x 10^5 cells per well) were grown to sub-confluence and co-transfected with 20 ng of the pmirGLO constructs, 20 ng normalizing ß-Galactosidase plasmid (Applied Biosystem) and 100 nM of precursor *hsa-miR-632* or a pre-miR negative control (Ambion)

using lipofectamine 2000 (Invitrogen) (18). Luminescence was measured 24h after transfection on a Synergy HT device (Biotech) using Luciferase Assay System (Promega). Firefly luciferase activity was normalized to β-Galactosidase activity (β-Galactosidase Enzyme Assay System, Promega) for each sample. All transfections were performed in quadruplicate, and each construct was tested in at least three independent transfections.

Supplemental References

1. Xu J, et al. Deletion of the chloride transporter Slc26a9 causes loss of tubulovesicles in parietal cells and impairs acid secretion in the stomach. *Proc Natl Acad Sci USA.* 2008;105(46):17955-60.

2. Anagnostopoulou P, Dai L, Schatterny J, Hirtz S, Duerr J, Mall MA. Allergic airway inflammation induces a pro-secretory epithelial ion transport phenotype in mice. *Eur Respir J.* 2010;36(6):1436-47.

3. Grubb BR, Paradiso AM, Boucher RC. Anomalies in ion transport in CF mouse tracheal epithelium. *Am J Physiol.* 1994;267(1 Pt 1):C293-C300.

4. Mall M, Bleich M, Greger R, Schreiber R, Kunzelmann K. The amiloride inhibitable Na^+ conductance is reduced by CFTR in normal but not in cystic fibrosis airways. *J Clin Invest.* 1998;102(1):15-21.

5. Ma T, et al. Thiazolidinone CFTR inhibitor identified by high-throughput screening blocks cholera toxin-induced intestinal fluid secretion. *J Clin Invest.* 2002;110(11):1651-8.

6. Mall M, et al. Activation of ion secretion via proteinase-activated receptor-2 in human colon. *Am J Physiol Gastrointest Liver Physiol.* 2002;282(2):G200-G210.

7. Mall MA, et al. Development of chronic bronchitis and emphysema in β-epithelial Na^+ channel-overexpressing mice. *Am J Respir Crit Care Med.* 2008;177(7):730-42.

8. Harkema JR, Plopper CG, Hyde DM, St George JA. Regional differences in quantities of histochemically detectable mucosubstances in nasal, paranasal, and nasopharyngeal epithelium of the bonnet monkey. *J Histochem Cytochem.* 1987;35(3):279-86.

9. Zhou Z, et al. Preventive but not late amiloride therapy reduces morbidity and mortality of lung disease in βENaC-overexpressing mice. *Am J Respir Crit Care Med.* 2008;178(12):1245-56.

10. Pfaffl MW. A new mathematical model for relative quantification in real-time RT-PCR. *Nucleic Acids Res.* 2001;29(9):E45.

11. Moffatt MF, et al. Genetic variants regulating ORMDL3 expression contribute to the risk of childhood asthma. *Nature.* 2007;448(7152):470-3.

12. Michel S, et al. Unifying candidate gene and GWAS Approaches in Asthma. *PLoS ONE.* 2010;5(11):e13894.

13. Weiland SK, et al. Prevalence of respiratory and atopic disorders among children in the East and West of Germany five years after unification. *Eur Respir J.* 1999;14(4):862-70.

14. Li Y, Willer CJ, Ding J, Scheet P, Abecasis GR. MaCH: using sequence and genotype data to estimate haplotypes and unobserved genotypes. *Genet Epidemiol.* 2010;34(8):816-34.

15. The International HapMap Project. *Nature.* 2003;426(6968):789-96.

16. Lohi H, et al. Functional characterization of three novel tissue-specific anion exchangers SLC26A7, -A8, and -A9. *J Biol Chem.* 2002;277(16):14246-54.

17. Wang J, Pitarque M, Ingelman-Sundberg M. 3'-UTR polymorphism in the human CYP2A6 gene affects mRNA stability and enzyme expression. *Biochem Biophys Res Commun.* 2006;340(2):491-7.

18. Thum T, et al. MicroRNA-21 contributes to myocardial disease by stimulating MAP kinase signalling in fibroblasts. *Nature.* 2008;456(7224):980-4.

19. Barrett JC, Fry B, Maller J, Daly MJ. Haploview: analysis and visualization of LD and haplotype maps. *Bioinformatics.* 2005;21(2):263-5.

Supplemental Figures

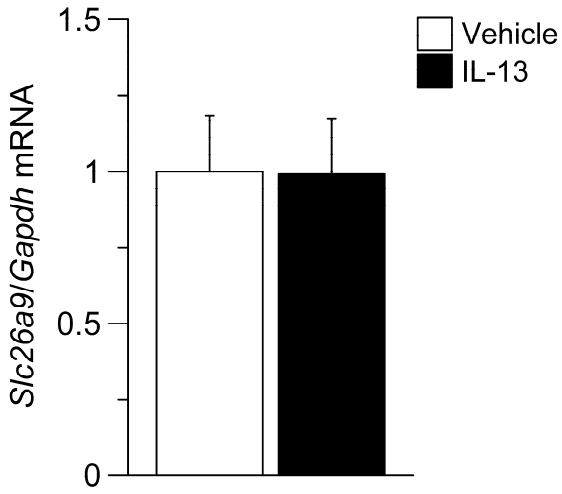

Supplemental Figure 1. Transcript expression of *Slc26a9* in mouse airways. Expression levels of *Slc26a9* mRNA in freshly excised native airway tissues from vehicle- and IL-13 treated wild-type mice. Results are expressed as relative fold changes from vehicle-treated wild-type mice. Data represent mean ± SEM (*n* = 7-13 mice per group).

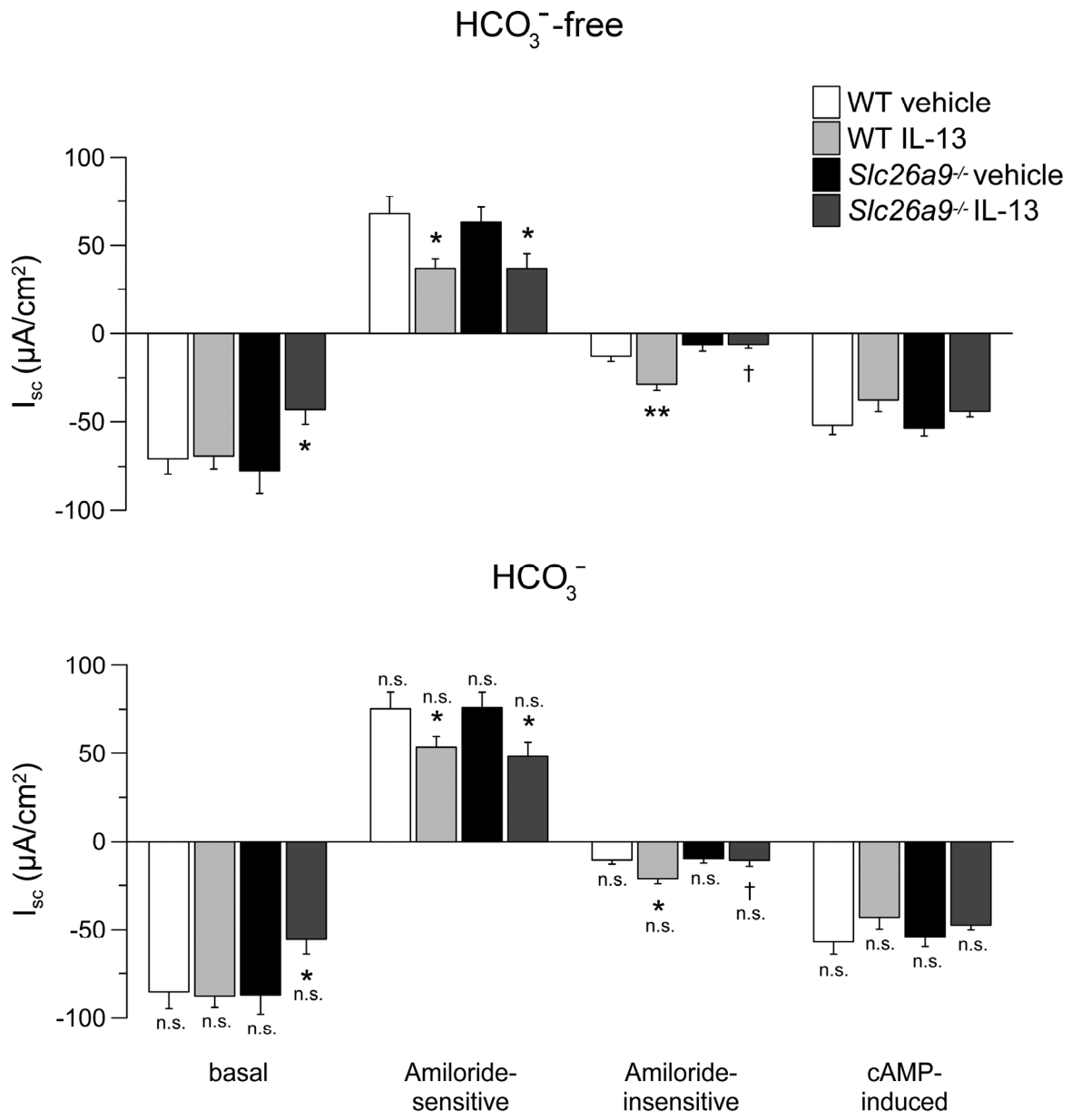

Supplemental Figure 2. HCO_3^- has no effect on ion transport in bronchi from wild-type and *Slc26a9*$^{-/-}$ mice. Comparison of basal short circuit current (I_{sc}), amiloride-sensitive I_{sc}, amiloride-insensitive I_{sc} and cAMP-induced I_{sc} in the absence (upper panel) and presence of HCO_3^- (lower panel) in freshly excised bronchial tissues from vehicle-treated and IL-13 treated wild-type and *Slc26a9*$^{-/-}$ mice. Data represent mean ± SEM (*n* = 5-11 mice per group). **P* < 0.05, ***P* < 0.01 compared with vehicle-treated mice of the same genotype. $^{\dagger}P$ < 0.05 compared with IL-13 treated wild-type mice. n.s., not significant compared with same genotype and treatment group in the absence of HCO_3^-.

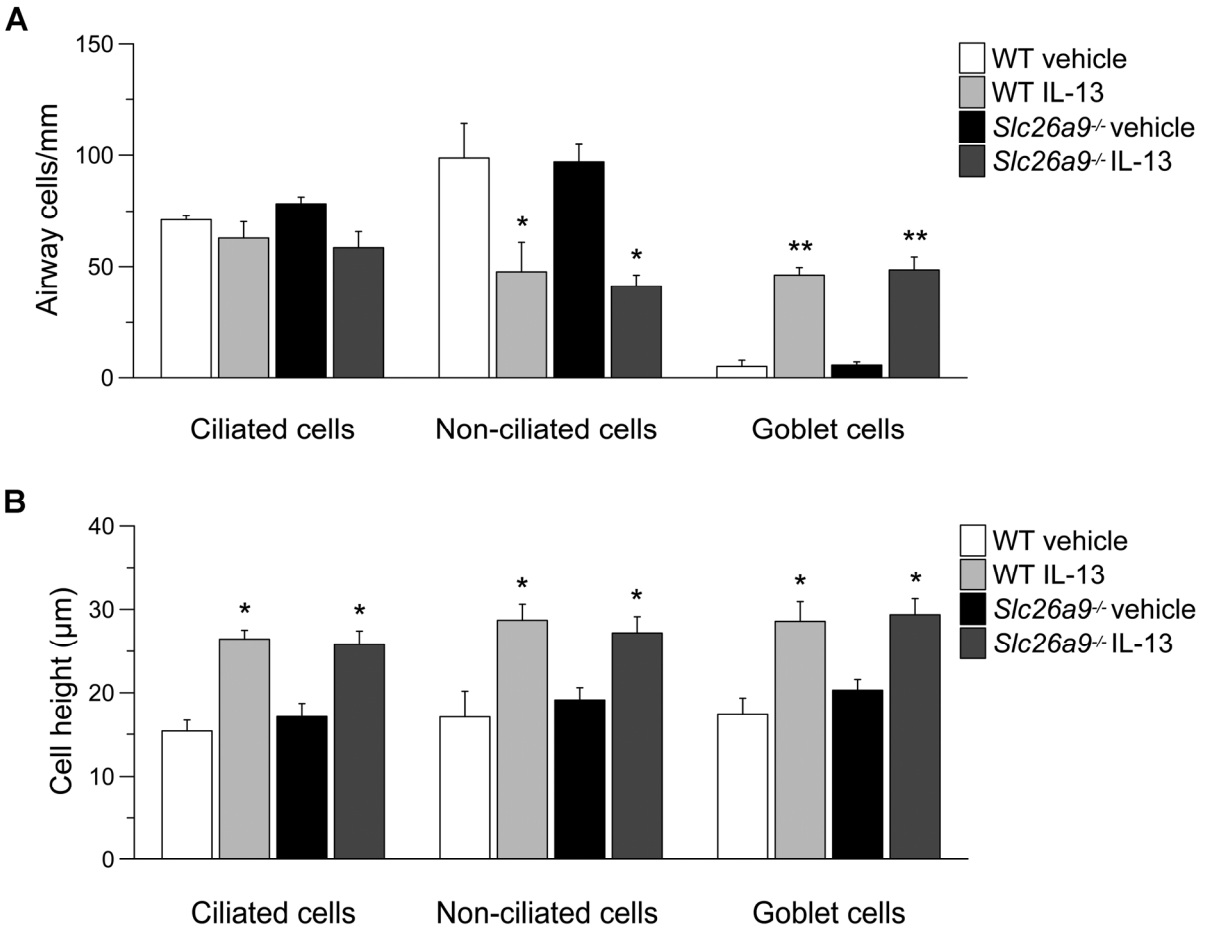

Supplemental Figure 3. IL-13 induces goblet cell metaplasia and epithelial cell hypertrophy in bronchi from wild-type and *Slc26a9*$^{-/-}$ mice. (A,B) Summary of numeric densities (A) and cell height (B) of ciliated cells, non-ciliated Clara cells and goblet cells in proximal main axial airways from vehicle-treated and IL-13 treated wild-type and *Slc26a9*$^{-/-}$ mice. Data represent mean ± SEM (n = 4-11 mice for each group). *P < 0.05, **P < 0.01 compared with vehicle-treated mice of the same genotype.

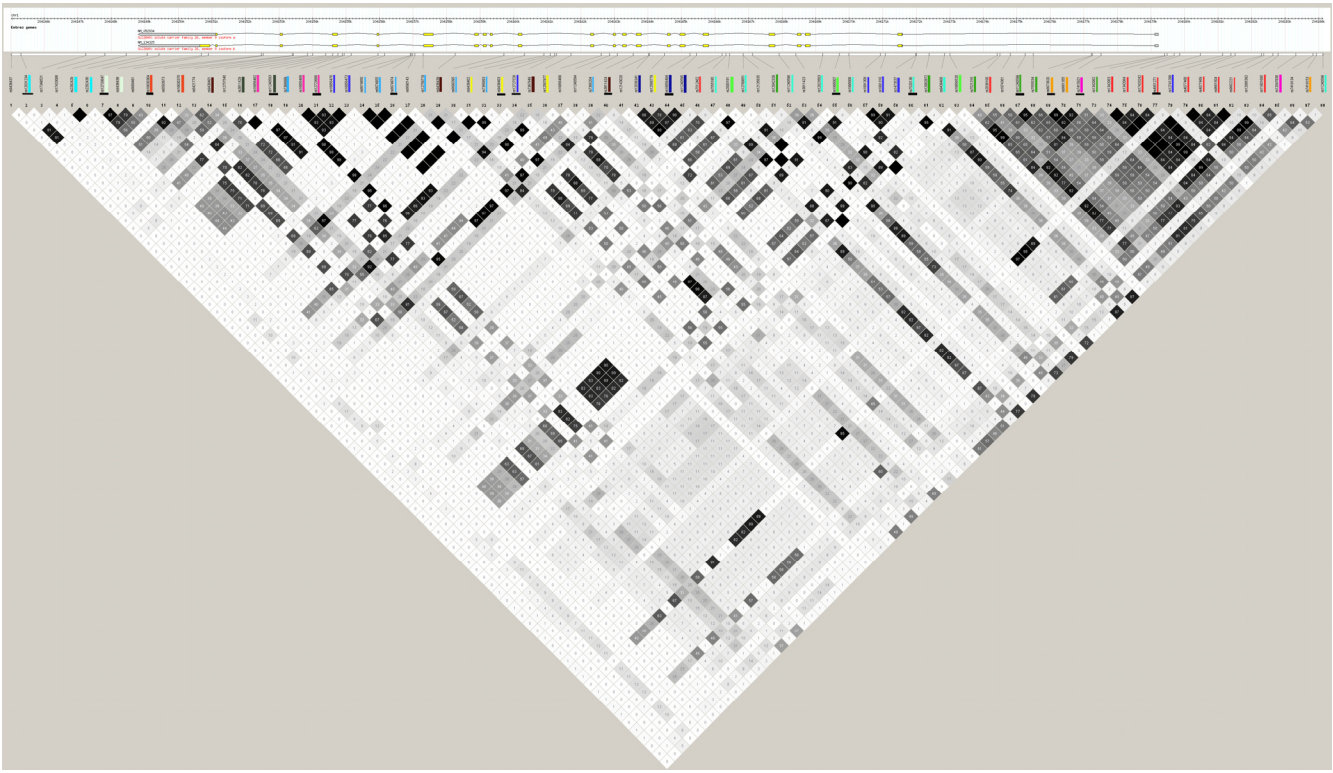

Supplemental Figure 4. Linkage disequilibrium and gene structure of the human *SLC26A9* gene on chr 1. Linkage disequilibrium (LD) between all SNPs of *SLC26A9* including ± 10kb borders was calculated and presented by the Haploview software 4.2 (19). Genotyping and imputation data were combined for LD analysis and the gene structure was downloaded from the HapMap database. All SNPs grouped together in one bin by the Haploview tagging algorithm were underlined with the same colour for a better visualisation. Tagging SNPs mentioned in Supplemental Table 1 were marked with an additional black bar.

Supplemental Table 1

Association between polymorphisms in the *SLC26A9* gene and childhood asthma (n=1361; asthmatics n=661) in an additive model providing odds ratios (OR) and 95% confidence intervals

Tagging Bin	Tagging SNP (Nr in LD-plot)*	Variations captured (BIN)	Tested allele	MAF	Odds ratio (CI 95%)	*P*
1	rs9438437 (1)	rs9438437	C	0.02	0.85 (0.50-1.47)	0.571
2	rs12031234 (2)	rs12031234, rs2282429, rs2282430	T	0.07	1.48 (1.09-2.00)	0.012
3	rs17348521 (3)	rs17348521	T	0.07	1.01 (0.75-1.35)	0.967
4	rs17433088 (4)	rs17433088	C	0.18	0.96 (0.79-1.18)	0.717
5	rs12733647 (7)	rs12733647, rs9438438	T	0.10	0.85 (0.66-1.10)	0.221
6	rs6669481 (9)	rs6669481	C	0.11	0.92 (0.73-1.18)	0.520
7	rs16830364 (10)	rs16830370, rs16830364	G	0.08	0.83 (0.63-1.10)	0.191
8	rs6593973 (11)	rs6593973	A	0.12	0.86 (0.68-1.08)	0.194
9	rs6421774 (13)	rs6421774	C	0.23	0.85 (0.71-1.02)	0.085
10	rs12757540 (15)	rs12757540	A	0.14	0.83 (0.67-1.04)	0.114
11	rs11240593 (18)	rs3811429, rs11240593	C	0.09	1.22 (0.93-1.60)	0.159
12	rs12723666 (21)	rs12723666, rs16856468, rs16856462	A	0.10	0.84 (0.65-1.09)	0.199
13	rs6674874 (26)	rs6674874, rs7366204, rs12759719, rs6690395, rs7366689, rs6674855, rs7366893, rs6674850	C	0.09	0.92 (0.70-1.20)	0.519
14	rs6690143 (27)	rs6690143	C	0.00	2.68 (0.71-10.13)	0.148
15	rs9438403 (33)	rs12568779, rs9438402, rs12567977, rs9438403	A	0.07	1.18 (0.88-1.58)	0.275
16	rs12727528 (34)	rs1891309, rs12741299, rs16856470, rs1473537, rs1891310, rs16856473, rs12727528	A	0.09	0.79 (0.60-1.04)	0.089
17	rs16856489 (37)	rs16856489	A	0.05	0.96 (0.66-1.39)	0.831
18	rs11240594 (38)	rs11240594	A	0.16	0.94 (0.77-1.17)	0.594
19	rs3811424 (40)	rs9438401, rs7367849, rs9438439, rs3811424	A	0.30	0.92 (0.77-1.09)	0.320
20	rs12143020 (41)	rs12143020	T	0.04	1.00 (0.67-1.48)	0.982
21	rs16856494 (44)	rs11240595, rs12036341, rs16856494	T	0.09	1.02 (0.78-1.34)	0.866
22	rs12135835 (50)	rs12135835	A	0.05	1.18 (0.84-1.67)	0.348
23	rs3811423 (53)	rs3811423	T	0.25	0.92 (0.77-1.10)	0.371
24	rs1995007 (55)	rs2000181, rs16856520, rs1995007	A	0.01	0.90 (0.38-2.14)	0.818

25	rs7520136 (60)	rs12023503, rs11240599, rs1995006, rs11240596, rs12760651, rs7555185, rs9438406, rs7520136	C	0.10	0.95 (0.74-1.23)	0.714
26	rs1874361 (66)	rs1874361	A	0.43	1.02 (0.87-1.20)	0.791
27	rs11240598 (67)	rs1342062, rs7521316, rs7555534, rs12082872, rs12042328, rs11240598	C	0.34	1.05 (0.89-1.24)	0.534
28	rs6673820 (69)	rs7419153, rs6661355, rs6673820	A	0.43	1.00 (0.85-1.16)	0.951
29	rs4951271 (77)	rs4951271, rs1342063, rs9661504, rs7512462, rs11801695, rs1342064, rs2036100, rs4077469, rs4077468, rs9662221, rs17433242	G	0.45	0.97(0.83-1.14)	0.732
30	rs7415921 (77)	rs12047830, rs7415921	G	0.45	1.02 (0.87-1.18)	0.838
31	rs12095392 (83)	rs12095392	A	0.14	0.90 (0.72-1.13)	0.361
32	rs7419134 (86)	rs7419134	A	0.06	1.12 (0.82-1.54)	0.484
* if tagging SNP represents more than one SNP, position of all tagged SNPs is mentioned						